Nanoscale Advances

ROYAL SOCIETY OF CHEMISTRY

PAPER

View Article Online
View Journal | View Issue

Cite this: *Nanoscale Adv.*, 2022, **4**, 5070

Impact of fluorination on the energy level alignment of an $F_nZnPc/MAPbI_3$ interface†

Elham Oleiki, [a] Saqib Javaid[ab] and Geunsik Lee *[a]

We have studied interactions at an interface between a Methylammonium Lead Iodide ($MAPbI_3$) surface and zinc-phthalocyanine molecules with F substituting peripheral H (F_nZnPc; $n = 4$, 8, 12, and 16) by employing hybrid density functional theory (DFT) based simulations. These calculations show that F_nZnPc molecules form a stable interface with $MAPbI_3$, whose binding strength is comparable to that of the un-substituted (ZnPc) case. As a consequence of fluorination, an increase in the ionization potential/electron affinity (*i.e.*, a systematic lowering of molecular energy levels), as well as interfacial charge transfer, is observed whose magnitude depends upon the degree of fluorination. In contrast to the common belief of unfavorable hole transfer for excessive fluorination, our work unveils that the valence band offset remains favorable for all ranges of substitution (n); thus, hole transfer from $MAPbI_3$ to F_nZnPc is facilitated while the electron transfer process is suppressed. This unusual behavior originates from the intermolecular interaction and substrate-to-molecule electron transfer at the heterojunction, which gradually suppresses the downward shift of F_nZnPc energy levels by increasing the value of n. Given the beneficial impacts of fluorination, such as hydrophobicity, our work provides valuable insight for exploiting stable F_nZnPc towards high-efficiency perovskite solar cells.

Received 29th August 2022
Accepted 9th October 2022

DOI: 10.1039/d2na00582d

rsc.li/nanoscale-advances

Introduction

Within hybrid perovskite solar cells, searching for cheap, stable and efficient hole transport materials is one of the critical research areas.[1–3] At the moment, spiro-OMeTAD is commonly used as a hole transport layer (HTL).[4,5] However, spiro-OMeTAD is expensive and unstable under hot and humid conditions.[6] Thus, replacing spiro-OMeTAD is the key to developing durable and affordable solar cell technology. In this regards, metal-phthalocyanine molecules (MPc; M = 3d metal and Pc = $N_8C_{32}H_{16}$) are thermally stable and relatively cheap, and can easily be grown into ordered thin films.[7,8] Therefore, MPc molecules are widely used in organic solar cells as a donor material.[9] Previous studies have confirmed that MPc can readily be utilized as a HTL with efficiency approaching ~20%.[10–12] Later, DFT based calculations further elucidated the interface electronic structure, where a suitable energy level alignment for hole transfer was found for face-on orientation.[13,14]

Recently, it has been shown that halogenated molecular materials offer an excellent choice as a hole selective layer or HTL.[1,2,15,16] Halogenation allows for efficient interfacial charge (hole) transfer *via* tailoring favorable energy level alignment. Moreover, the presence of halogen bonds at the interface passivates surface/interface defects, which in turn suppresses the recombination and thus improves the device stability. The halogenation of MPc can also be performed by substituting peripheral H atoms with fluorine (F), resulting in fluorinated metal-phthalocyanine.[17,18] The F concentration (*i.e.*, F/H ratio) within the MPc molecule can be readily controlled (*i.e.*, F_nMPc; $n = 1$–16), which facilitates suitable energy level tuning for the perspective applications.[19] Indeed, F_nMPc is employed extensively for different applications such as gas sensing and molecular electronics/spintronics.[20–22] The integration of F_nMPc within a perovskite solar cell can be very advantageous; F_nMPc contains a highly hydrophobic C–F bond, which will impede the well-known moisture-related degradation of $MAPbI_3$.[23,24] Furthermore, as shown previously, the presence of F (*via* C–F bond within fluorinated graphene) at the interface can help to passivate the grain and surface defects of $MAPbI_3$, thus improving the device performance and stability.[25] This approach has recently been validated experimentally in the case of structurally similar porphyrin molecules, where fluorination significantly enhanced the stability and efficiency of photovoltaic devices.[16] However, the utilization of F_nMPc within hybrid solar cells is contingent upon suitable energy level alignment with $MAPbI_3$ for an efficient charge separation process.

In this work, we have studied an interface between the $MAPbI_3$ surface and fluorinated Zn-phthalocyanine (F_nZnPc) by employing DFT based simulations. Specifically, four different degrees of fluorinations are investigated, *i.e.*, F_4ZnPc, F_8ZnPc,

[a]*Department of Chemistry, Ulsan National Institute of Science and Technology (UNIST), Ulsan 44919, Republic of Korea. E-mail: gslee@unist.ac.kr*

[b]*MMSG, Theoretical Physics Division, PINSTECH, P.O. Nilore, Islamabad, Pakistan*

† Electronic supplementary information (ESI) available. See DOI: https://doi.org/10.1039/d2na00582d

F_{12}ZnPc, and (fully fluorinated) F_{16}ZnPc. These calculations show that despite lowering molecular energy levels due to fluorination, all the fluorinated compounds including F_{16}ZnPc exhibit an interfacial energy level alignment suitable for hole transfer (and electron blockage) from $MAPbI_3$ to F_nZnPc.

Computational methods

All DFT calculations have been performed by employing the VASP suite, which is based on the plane wave pseudopotential approach.[26] Generalized gradient approximation (GGA) within PBE parameterization was utilized as an exchange correlation functional.[27] Furthermore, van der Waals (vdW) interactions were incorporated by adding dispersion correction to the total energy and forces by employing the Tkatchenko and Scheffler (TS) approach.[28] The electronic structure and band gaps were further improved by utilizing the HSE06 hybrid functional including spin–orbit coupling,[29] which is necessary for correct estimation of the $MAPbI_3$ electronic structure.

To model the $MAPbI_3$ surface, a room temperature tetragonal phase is considered with experimentally determined lattice parameters, *i.e.*, $a = b = 8.856$ Å and $c = 12.65$ Å.[30] Specifically, an energetically optimum $MAPbI_3$ (001) surface was used with a plane periodicity of 2×2 and having PbI_2 termination.[31,32] A vacuum layer of ~15 Å was provided to avoid spurious interactions between the periodic images. The kinetic energy cutoff was set to 400 eV, while convergence criteria of 10^{-5} eV and 0.015 eV $Å^{-1}$ were employed for energies and forces, respectively. A single Γ-point is used for *k*-point sampling, providing converged results for the electronic structure.[14] The binding energy (E_B) is defined as:

$$E_B = E(MAPbI_3) + E(F_nZnPc) - E(MAPbI_3/F_nZnPc) \quad (1)$$

where $E(MAPbI_3/F_nZnPc)$, $E(MAPbI_3)$, and $E(F_nZnPc)$ correspond to the total energies of the combined $MAPbI_3/F_nZnPc$ system, $MAPbI_3$ slab, and isolated F_nZnPc molecule, respectively. As per this definition, a positive (negative) value of E_B suggests a stable (unstable) interface. Finally, to find stable structures for F_nZnPc, different possible positions of F ions on the molecular periphery were considered. The structurally optimum structures thus obtained are shown in the ESI (Fig. S1†).

Results and discussion

Table 1 describes the adsorption properties of F_nZnPc on the $MAPbI_3$ surface, namely, the adsorption site, adsorption distance, and binding energy as a function of the fluorination level. For adsorption sites, three high symmetry positions are considered, which are referenced with respect to the position of the Zn atom on the $MAPbI_3$ surface, *i.e.*, Pb top (Pb_{top}), I top (I_{top}), and bridge position between the I and Pb atoms of $MAPbI_3$. For all F_nZnPc molecules, I_{top} is found to be the energetically optimum adsorption position with an adsorption energy of 2.4–2.6 eV (Table 1). We note that the energetic difference between I top and bridge positions is rather small, though this difference is significantly larger for optimum I top and Pb top positions (Table S1†). This is in contrast to the case of unsubstituted ZnPc, where differences between all adsorption positions were rather small and their energies were comparable.[14] Furthermore, a gradual reduction in the molecule-surface separation is observed with fluorination; the adsorption distance for F_{16}ZnPc is 2.84 Å as compared to 2.98 Å for ZnPc. However, fluorination does not bring about a significant variation to the binding energies in comparison to that of unsubstituted ZnPc, whose binding energy was about 2.5–2.6 eV.[14]

Table 1 Most stable adsorption site, associated adsorption distance (*d*), and binding energy (E_B) of fluorinated phthalocyanine molecules on $MAPbI_3$(001). The adsorption site is referenced with respect to the position of the Zn atom

	Site	*d* (Å)	E_B (eV)
ZnPc	I_{top}/Pb_{top}	2.98	2.54
F_4ZnPc	I_{top}	2.91	2.50
F_8ZnPc	I_{top}	2.89	2.40
F_{12}ZnPc	I_{top}	2.84	2.62
F_{16}ZnPc	I_{top}	2.84	2.46

The adsorption geometry is further elaborated in Fig. 1, which schematically depicts F_{16}ZnPc adsorption on the $MAPbI_3$ I_{top} position. As highlighted in previous work,[13,14] the planar conformation of unsubstituted ZnPc is significantly distorted on the $MAPbI_3$ surface. In particular, peripheral H atoms move towards the surface such that a large vertical downshift of 0.45 Å is observed for H with respect to Zn. In contrast, this vertical distortion is much less pronounced in F_nZnPc. For example, the maximum vertical distance between peripheral F and Zn is reduced to 0.16 Å for F_{16}ZnPc. Nevertheless, the fluorinated case has greater distortion energy of the adsorbate or substrate due to the adsorbate–substrate coupling with respect to the separated equilibrium structure (eqn. S(1)), where the total distortion energy is calculated to be 0.46 eV and 0.20 eV for F_{16}ZnPc/$MAPbI_3$ and ZnPc/$MAPbI_3$, respectively (Table S2†). Meanwhile, a gradual increase in charge transfer from $MAPbI_3$ to F_nZnPc is observed as the number of fluorine atoms increases. Specifically, a charge transfer of ~0.18, 0.25, 0.29, and 0.34 e is

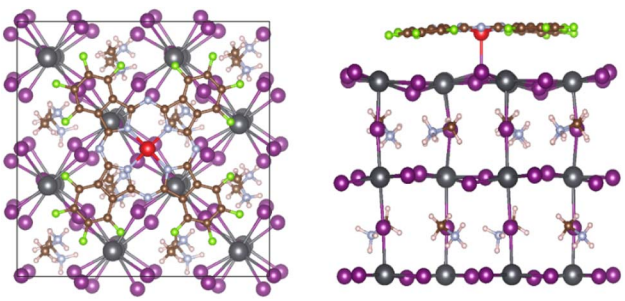

Fig. 1 Optimized structure of F_{16}ZnPc adsorbed on $MAPbI_3$(001), (left) top and (right) side views along [100]. The solid square in the top view denotes a 2×2 supercell of a tetragonal primitive cell. Atomic colour scheme: Pb (grey), I (purple), N (light blue), C (brown), H (white), Zn (red) and F (green).

observed for F_4ZnPc, F_8ZnPc, F_{12}ZnPc and F_{16}ZnPc, respectively, according to Bader charge analysis, while the magnitude of interfacial charge transfer is much smaller (~0.03 or 0.10 e) for ZnPc/$MAPbI_3$.[13] This gradual increase of charge transfer with fluorination is associated with the higher electronegativity of F than H. Such charge transfer from the substrate to F_{16}ZnPc could give rise to stronger electrostatic attraction between them with respect to the case without fluorination. However, upon fluorination, the electrostatic energy gain is impeded by a greater distortion energy (~0.26 eV) as there was no significant difference in the calculated adsorption energies of F_{16}ZnPc and ZnPc.

Fig. 2 presents the electronic structure of the F_nZnPc/$MAPbI_3$ interface, where the partial density of states (PDOS) is depicted as a function of the fluorination level. Overall, the electronic structure of $MAPbI_3$ and F_nZnPc does not seem to vary significantly due to interfacial interactions. This is understandable since direct hybridization between F_nZnPc and $MAPbI_3$ is relatively weak as discussed above. Nevertheless, an important trend is observed; a gradual downward shift of the PDOS of F_nZnPc with increasing n is observed with respect to that of $MAPbI_3$. Indeed, going from F_4ZnPC to F_{16}ZnPc, both the HOMO and LUMO of phthalocyanine molecules (which are dominated by C atoms) are pushed to lower energies by ~0.45 eV. This effect is further demonstrated in Fig. 3, where

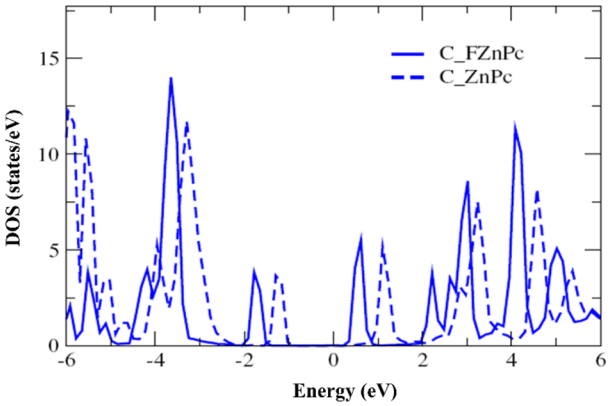

Fig. 3 Comparison of the molecular C PDOS for F_{16}ZnPc/$MAPbI_3$(001) (solid line, C_FZnPc) and ZnPc/$MAPbI_3$(001) (dashed line, C_ZnPc) by adjusting the two vacuum levels to be equal to each other. The positive and negative energy values indicate the unoccupied and occupied states, respectively.

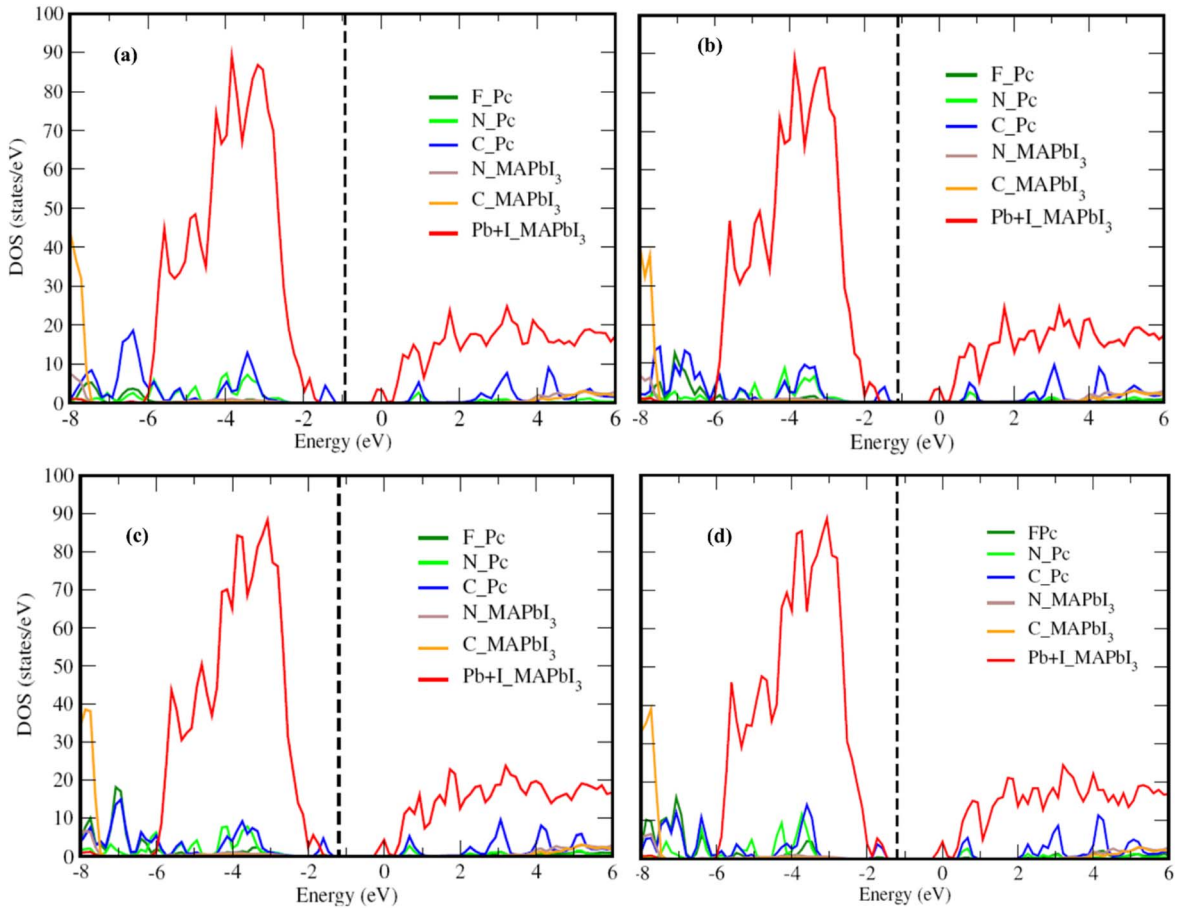

Fig. 2 Partial density of states (PDOS) of the interface between $MAPbI_3$(001) and (a) F_4ZnPc, (b) F_8ZnPc, (c) F_{12}ZnPc and (d) F_{16}ZnPc. All calculations were performed with the HSE06 plus spin–orbit coupling approach. Dashed vertical line represents the Fermi level. The contributions of F, N, and C atoms of F_nZnPc are given by F_Pc, N_Pc, and C_Pc, respectively, and N_$MAPbI_3$, C_$MAPbI_3$, and Pb + I_$MAPbI_3$ denote the contributions of N, C, and sum of Pb and I, respectively, of $MAPbI_3$.

the molecular C PDOSs are plotted together for F_{16}ZnPc/$MAPbI_3$ and ZnPc/$MAPbI_3$ such that their vacuum levels are aligned. Evidently, both the HOMO and LUMO of F_{16}ZnPc are shifted downward by ~0.55 eV compared to that of ZnPc.

The attachment of an electron withdrawing element like F in place of H is expected to lower both the HOMO and LUMO resulting in an increase in both the ionization potential and electron affinity, as observed in Fig. 2 and 3.[33] Indeed, fluorination is used to induce n-type transport within phthalocyanine molecules, which otherwise exhibit p-type behavior.[17] The key impact of the environmental coupling (*i.e.*, underlying $MAPbI_3$ surface) is a noticeable reduction in this downward shift of energy levels. For example, the HOMO level shifts down by ~0.9 eV from bare ZnPc to bare F_{16}ZnPc, which is reduced to ~0.55 eV after adsorption on the $MAPbI_3$ surface. This reduction is likely to eliminate the concern of too much fluorination causing an F_nZnPc HOMO level lying below the valence band maximum (VBM) of $MAPbI_3$. The origin of such advantageous properties is studied with additional PBE calculations for the environmental effect on the molecular HOMO level. As shown in Fig. 4a, the energy level of the ZnPc HOMO is calculated to be −5.0 eV with respect to the vacuum level for the isolated case, whereas it is −5.33 eV for the adsorbed case on $MAPbI_3$, and thus the ZnPc HOMO level is lowered by 0.33 eV upon adsorption. In addition, for ZnPc/MAPbI3, the second highest occupied orbital is from the substrate VBM and its energy level of −5.84 eV is very close to that of the pristine MAPbI3 surface (−5.82 eV). Similar results for F16ZnPc are shown in Fig. 4b. One can see that the molecular HOMO level rises upon adsorption from −5.69 to −5.57 eV; thus, it still remains above the substrate VBM (−5.77 eV). Hence our PBE results in Fig. 4a and b agree qualitatively well with the HSE06 results in Fig. 2 and 3, namely the downward shift of the ZnPc HOMO level upon fluorination is suppressed when the molecules are adsorbed.

We attribute the main reason to intermolecular and surface-molecular electrostatic interactions. Fig. 4c shows the HOMO levels of ZnPc (solid) and F_{16}ZnPc (dashed) additionally for two intermediate hypothetical environments displayed between the isolated (gas phase molecule at left most) and the adsorbed case (surface–molecule interaction at right most). For the first

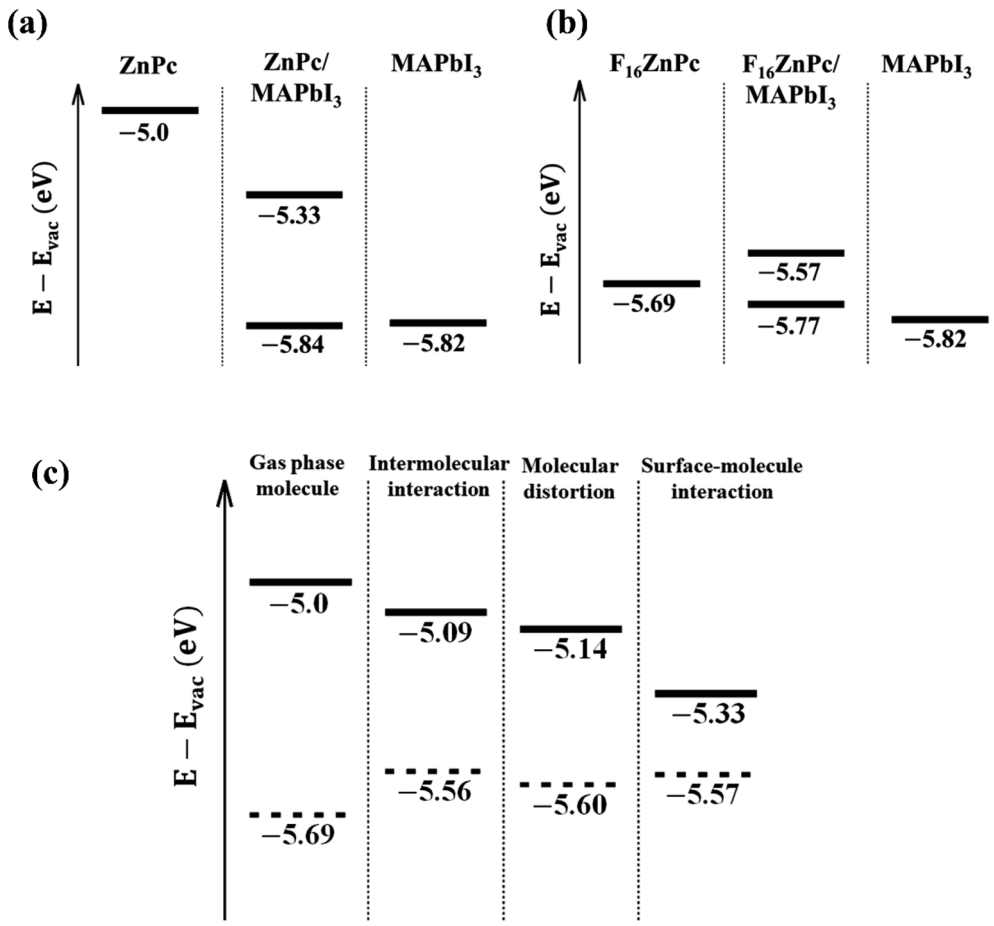

Fig. 4 The HOMO energy levels relative to the vacuum level for an equilibrium structure of the molecule (left most), $MAPbI_3$(001) substrate (rightest), or heterosystem (middle). (a and b) ZnPc and F_{16}ZnPc for the molecule, respectively. (c) Solid (dashed) horizontal lines show ZnPc (F_{16}ZnPc) HOMO energy levels relative to the vacuum level for the equilibrium structures of an isolated gas phase molecule (left most) and an adsorbed molecule (rightest). The effect of intermolecular interaction and molecular distortion on the HOMO is shown in the middle left and middle right, respectively. In the middle left, the gas molecules are arranged into a square lattice, and in the middle right, the non-planar distortion by the interaction with the substrate is additionally included.

environment checking the intermolecular interaction, we arranged the gas phase ZnPc or F_{16}ZnPc molecules into a square lattice, where the lattice constant is chosen such that the intermolecular distance (Fig. S2†) is equal to that of the adsorbed molecules (Fig. 1). From Fig. 4c, one can see that the lateral molecule–molecule interaction lowers or raises the HOMO level for ZnPc or F_{16}ZnPc, respectively, with respect to the isolated case. This opposite trend is caused by the positive (+28.8 ea_0^2) and negative (−36.0 ea_0^2) molecular quadrupole moments[34] in the case of hydrogen and fluorine as peripheral species. We note that similar intermediate behavior is also expected if different (*e.g.* axisymmetric) molecular structures are used for partially fluorinated molecules (Table S3, Fig. S3, and S4†). The second environment additionally includes the molecule distortion caused by the interaction with the substrate. We note that the surface PbI_2 layer has −0.98 e Bader charge, and thus relatively positive peripheral hydrogen atoms of ZnPc or central atoms including Zn of F_{16}ZnPc tilt down to the substrate. Such slight derivation from the perfect planar shape makes the HOMO level further lower for two cases, as shown in the third panel indicated by molecular distortion in Fig. 4c. Finally, the presence of the substrate turns out to lower the HOMO level significantly for ZnPc; whereas it makes it a little higher for F_{16}ZnPc, mainly due to repulsive potential from additional electrons transferred from the substrate to the molecule. The magnitude of the HOMO level downward shift is in the order of F_4ZnPc > F_8ZnPc > F_{12}ZnPc (Fig. S5†).

Based on the electronic structure discussed above, Fig. 5 depicts the interfacial energy level alignment between the VBM of $MAPbI_3$ and the HOMO of F_nZnPc, which is important for understanding the impact of fluorination on the charge (hole/electron) transfer process. For comparison, the corresponding HOMO level of unsubstituted ZnPc is also shown. As shown in Fig. 3, the ionization potential of F_nZnPc increases due to fluorination. Most crucially, despite the downward shift of the HOMO, the energy level alignment remains favorable for hole transfer from $MAPbI_3$ to F_nZnPc since the molecular HOMO level is placed above the VBM of $MAPbI_3$. In particular, a sizeable energy level offset (ΔVBM) is present for F_4ZnPc, F_8ZnPc, and F_{12}ZnPc, which should facilitate the interfacial hole transfer. However, for the fully fluorination case (F_{16}ZnPc), the band offset is almost zero. This means that the hole transfer process will be feasible though not necessarily efficient.

These findings clearly show that the adsorption of F_nZnPc on $MAPbI_3$ leads to the formation of a stable interface, whose adsorption energy is comparable to that of its unsubstituted counterpart, *i.e.*, ZnPc/$MAPbI_3$ interface. The presence of the hydrophobic C–F bonds at the F_nZnPc/$MAPbI_3$ interface will impede the moisture-related degradation of $MAPbI_3$ and may also help to passivate surface defects, as is shown for other halogenated molecules.[24] Moreover, the electronic structure (Fig. 3) and interfacial valence level alignment (Fig. 5) demonstrate that the hole transfer from $MAPbI_3$ to F_nZnPc is feasible, while the alignment of conduction bands ensures electron blockage. In particular, for a relatively low substitution level of F (*e.g.*, F_4ZnPc), the valence band offset is appreciable, which should facilitate the hole transfer process while inhibiting the electron transfer simultaneously. It should be further pointed

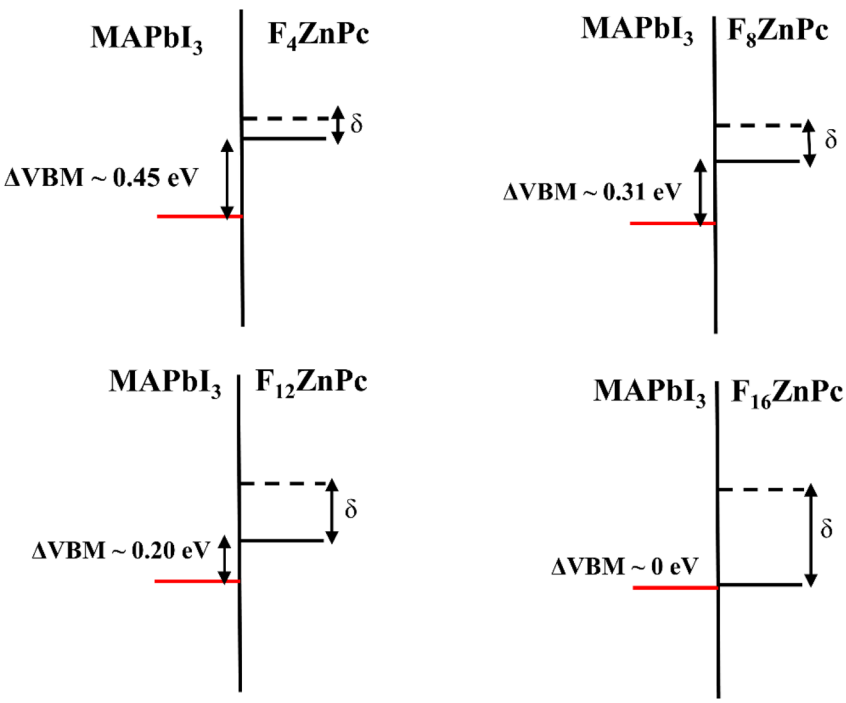

Fig. 5 Interfacial energy level alignment between the VBM of $MAPbI_3$ (red horizontal line) and the HOMO of F_nZnPc (black solid horizontal line). Dashed horizontal line represents the HOMO of unfluorinated ZnPc. As the fluorine content increases, the ionization potential of F_nZnPc increases as compared to unfluorinated ZnPc as highlighted by an increase in '*δ*'. Concomitantly, the valence band offset (ΔVBM) between F_nZnPc and $MAPbI_3$ gradually reduces.

out that the hole mobility of F_4ZnPc has the same order of magnitude as that of ZnPc in the bulk heterojunction system, while an increase in ionization potential due to fluorination may increase the open circuit voltage (V_{oc}), which will improve the overall efficiency of the device.[16,21] The comparable hole mobilities of ZnPc and F_nZnPc are in agreement with our band structure calculations (Fig. S6†).

Finally, as highlighted in Fig. 5, the HOMO of unsubstituted ZnPc lies at higher energy than that of F_nZnPc such that the hole transfer is feasible from F_nZnPc to ZnPc. This means that besides the hole transport medium, a heterojunction ($MAPbI_3$/F_nZnPc/ZnPc) can be formed, where a protective and hole selective interface layer of F_nZnPc can be deposited between $MAPbI_3$ and a usual hole transport layer such as ZnPc. Also, from an experimental report,[35] the degree of crystallinity is lowered for fluorinated ZnPc compared to that of unsubstituted ZnPc and the roughness of F_4ZnPc is two times smaller than that of ZnPc, and hence the junction interface will become smooth due to the presence of F_nZnPc towards a better electronic contact. There might be a deteriorating effect like carrier trapping caused by the F_nZnPc/ZnPc interface, but the impact is not significant and rather provides a way of tuning the ionization energy continuously.[34,36] Overall, the presence of F_nZnPc as an interlayer or hole transport medium will improve the stability of solar cell devices against moisture and the hole extraction efficiency.

Conclusions

We have studied interactions at an F_nZnPc/$MAPbI_3$ interface by employing DFT based simulations. The results show that F_n-ZnPc forms a stable interface with the $MAPbI_3$ surface with binding energies comparable to that of the unsubstituted case. The alignment between the $MAPbI_3$ VBM and F_nZnPc HOMO at the interface promotes hole transfer from $MAPbI_3$ to F_nZnPc, while impeding the deleterious electron transfer process simultaneously. These results suggest that incorporating F_n-ZnPc into photovoltaic devices as a protective interlayer or as a hole transport medium should significantly improve the device stability without any noticeable reduction in the efficacy, particularly for lower level F substitution (*e.g.*, F_4ZnPc and F_8ZnPc).

Conflicts of interest

There are no conflicts to declare.

Acknowledgements

This work was supported by the National Research Foundation of Korea (NRF) grant funded by the Korean government (MSIT) (No. NRF-2021M3H4A1A02055684) and Pakistan Atomic Energy commission. We also acknowledge the support of MIS at PIN-STECH, and PIEAS, Islamabad, regarding providing the computational resources. GL acknowledges support of Samsung Electronics Co. through Industry-University Cooperation Project (IO221012-02835-01).

References

1 A. Al-Ashouri, E. Köhnen, B. Li, A. Magomedov, H. Hempel, P. Caprioglio, J. A. Márquez, A. B. Morales Vilches, E. Kasparavicius, J. A. Smith, N. Phung, D. Menzel, M. Grischek, L. Kegelmann, D. Skroblin, C. Gollwitzer, T. Malinauskas, M. Jošt, G. Matič, B. Rech, R. Schlatmann, M. Topič, L. Korte, A. Abate, B. Stannowski, D. Neher, M. Stolterfoht, T. Unold, V. Getautis and S. Albrecht, *Science*, 2020, **370**, 1300–1309.
2 N. J. Jeon, H. Na, E. H. Jung, T.-Y. Yang, Y. G. Lee, G. Kim, H.-W. Shin, S. Il Seok, J. Lee and J. Seo, *Nat. Energy*, 2018, **3**, 682–689.
3 L. Canil, J. Salunke, Q. Wang, M. Liu, H. Köbler, M. Flatken, L. Gregori, D. Meggiolaro, D. Ricciarelli, F. De Angelis, M. Stolterfoht, D. Neher, A. Priimagi, P. Vivo and A. Abate, *Adv. Energy Mater.*, 2021, **11**, 2101553.
4 D. Meggiolaro, E. Mosconi, A. H. Proppe, R. Quintero-Bermudez, S. O. Kelley, E. H. Sargent and F. De Angelis, *ACS Energy Lett.*, 2019, **4**, 2181–2184.
5 Y. Li, H. Li, C. Zhong, G. Sini and J.-L. Brédas, *npj Flexible Electron.*, 2017, **1**, 2.
6 Y. Matsuo, K. Ogumi, I. Jeon, H. Wang and T. Nakagawa, *RSC Adv.*, 2020, **10**, 32678–32689.
7 M. Grobosch, C. Schmidt, R. Kraus and M. Knupfer, *Org. Electron.*, 2010, **11**, 1483–1488.
8 H. Yamada, T. Shimada and A. Koma, *J. Chem. Phys.*, 1998, **108**, 10256–10261.
9 A. A. A. Torimtubun, J. Follana-Berná, J. G. Sánchez, J. Pallarès, Á. Sastre-Santos and L. F. Marsal, *ACS Appl. Energy Mater.*, 2021, **4**, 5201–5211.
10 G. Yang, Y.-L. Wang, J.-J. Xu, H.-W. Lei, C. Chen, H.-Q. Shan, X.-Y. Liu, Z.-X. Xu and G.-J. Fang, *Nano Energy*, 2017, **31**, 322–330.
11 Y. C. Kim, T.-Y. Yang, N. J. Jeon, J. Im, S. Jang, T. J. Shin, H.-W. Shin, S. Kim, E. Lee, S. Kim, J. H. Noh, S. I. Seok and J. Seo, *Energy Environ. Sci.*, 2017, **10**, 2109–2116.
12 T. Duong, J. Peng, D. Walter, J. Xiang, H. Shen, D. Chugh, M. Lockrey, D. Zhong, J. Li, K. Weber, T. P. White and K. R. Catchpole, *ACS Energy Lett.*, 2018, **3**, 2441–2448.
13 H. Qin, L. Xu and D. Zhong, *J. Phys. Chem. C*, 2020, **124**, 5167–5173.
14 S. Javaid and G. Lee, *RSC Adv.*, 2021, **11**, 31776–31782.
15 A. Ullah, K. H. Park, H. D. Nguyen, Y. Siddique, S. F. A. Shah, H. Tran, S. Park, S. I. Lee, K. Lee, C. Han, K. Kim, S. Ahn, I. Jeong, Y. S. Park and S. Hong, *Adv. Energy Mater.*, 2022, **12**, 2103175.
16 R. Azmi, U.-H. Lee, F. T. A. Wibowo, S. H. Eom, S. C. Yoon, S.-Y. Jang and I. H. Jung, *ACS Appl. Mater. Interfaces*, 2018, **10**, 35404–35410.
17 K. Shati, S. Javaid, R. T. A. Khan and M. J. Akhtar, *J. Magn. Magn. Mater.*, 2020, **494**, 165775.
18 S. Lindner, M. Knupfer, R. Friedrich, T. Hahn and J. Kortus, *Phys. Rev. Lett.*, 2012, **109**, 027601.
19 A. Varotto, C.-Y. Nam, I. Radivojevic, J. P. C. Tomé, J. A. S. Cavaleiro, C. T. Black and C. M. Drain, *J. Am. Chem. Soc.*, 2010, **132**, 2552–2554.

20 P. F. Siles, T. Hahn, G. Salvan, M. Knupfer, F. Zhu, D. R. T. Zahn and O. G. Schmidt, *Nanoscale*, 2016, **8**, 8607–8617.
21 J. Meiss, A. Merten, M. Hein, C. Schuenemann, S. Schäfer, M. Tietze, C. Uhrich, M. Pfeiffer, K. Leo and M. Riede, *Adv. Funct. Mater.*, 2012, **22**, 405–414.
22 D. Klyamer, A. Sukhikh, S. Gromilov, P. Krasnov and T. Basova, *Sensors*, 2018, **18**, 2141.
23 G.-H. Kim, H. Jang, Y. J. Yoon, J. Jeong, S. Y. Park, B. Walker, I.-Y. Jeon, Y. Jo, H. Yoon, M. Kim, J.-B. Baek, D. S. Kim and J. Y. Kim, *Nano Lett.*, 2017, **17**, 6385–6390.
24 S. Javaid, C. W. Myung, S. Pourasad, B. Rakshit, K. S. Kim and G. Lee, *J. Mater. Chem. A*, 2018, **6**, 18635–18640.
25 L. Yang, Y. Li, L. Wang, Y. Pei, Z. Wang, Y. Zhang, H. Lin and X. Li, *ACS Appl. Mater. Interfaces*, 2020, **12**, 22992–23001.
26 G. Kresse and J. Furthmüller, *Comput. Mater. Sci.*, 1996, **6**, 15–50.
27 J. P. Perdew, K. Burke and M. Ernzerhof, *Phys. Rev. Lett.*, 1996, **77**, 3865–3868.
28 A. Tkatchenko and M. Scheffler, *Phys. Rev. Lett.*, 2009, **102**, 073005.
29 A. V. Krukau, O. A. Vydrov, A. F. Izmaylov and G. E. Scuseria, *J. Chem. Phys.*, 2006, **125**, 224106.
30 S. T. A. G. Melissen, F. Labat, P. Sautet and T. Le Bahers, *Phys. Chem. Chem. Phys.*, 2015, **17**, 2199–2209.
31 G. Volonakis and F. Giustino, *J. Phys. Chem. Lett.*, 2015, **6**, 2496–2502.
32 J. H. Heo, S. H. Im, J. H. Noh, T. N. Mandal, C.-S. Lim, J. A. Chang, Y. H. Lee, H. Kim, A. Sarkar, M. K. Nazeeruddin, M. Grätzel and S. Il Seok, *Nat. Photonics*, 2013, **7**, 486–491.
33 J. E. Anthony, A. Facchetti, M. Heeney, S. R. Marder and X. Zhan, *Adv. Mater.*, 2010, **22**, 3876–3892.
34 M. Schwarze, K. S. Schellhammer, K. Ortstein, J. Benduhn, C. Gaul, A. Hinderhofer, L. Perdigón Toro, R. Scholz, J. Kublitski, S. Roland, M. Lau, C. Poelking, D. Andrienko, G. Cuniberti, F. Schreiber, D. Neher, K. Vandewal, F. Ortmann and K. Leo, *Nat. Commun.*, 2019, **10**, 2466.
35 D. D. Klyamer, A. S. Sukhikh, S. A. Gromilov, V. N. Kruchinin, E. V. Spesivtsev, A. K. Hassan and T. V. Basova, *Macroheterocycles*, 2018, **11**, 304–311.
36 M. Schwarze, W. Tress, B. Beyer, F. Gao, R. Scholz, C. Poelking, K. Ortstein, A. A. Günther, D. Kasemann, D. Andrienko and K. Leo, *Science*, 2016, **352**, 1446–1449.